Interplay of structure and transport properties of sodium-doped lanthanum manganite

2001 J. Phys.: Condens. Matter 13 9547

(http://iopscience.iop.org/0953-8984/13/42/314)

INSTITUTE OF PHYSICS PUBLISHING JOURNAL OF PHYSICS: CONDENSED MATTER

J. Phys.: Condens. Matter **13** (2001) 9547–9559 PII: S0953-8984(01)25675-6

Interplay of structure and transport properties of sodium-doped lanthanum manganite

S Roy, Y Q Guo, S Venkatesh and N Ali[1]

Department of Physics, Southern Illinois University, Carbondale, IL 62901-4401, USA

E-mail: nali@physics.siu.edu (N Ali)

Received 11 June 2001, in final form 23 July 2001
Published 5 October 2001
Online at stacks.iop.org/JPhysCM/13/9547

Abstract

The crystal structure, magnetic and electrical transport properties of the sodium-doped lanthanum manganites $La_{1-x}Na_xMnO_3$ ($0.07 \leqslant x \leqslant 0.40$) have been studied in detail using x-ray powder diffraction, atomic absorption spectroscopy, a SQUID (superconducting quantum interference device) magnetometer and the four-probe resistivity measurement technique. A rhombohedrally distorted perovskite structure has been observed in the range $0.07 \leqslant x \leqslant 0.20$. Both the lattice parameter and unit-cell volume decrease with increase in the Na content. A ferromagnetic-to-paramagnetic phase transition associated with a metal–insulator transition is observed for all the $La_{1-x}Na_xMnO_3$ compounds. There is a systematic change in both the Mn–O–Mn bond angle and the tolerance factor with Na content. The compositional variation of the magnetic and metal–insulator transition temperatures is explained as due to the distortion of the MnO_6 octahedron and increase in the tolerance factor that controls the hopping interaction. In the metallic region a $\rho \sim AT^2$ behaviour is observed due to the magnon excitation effect. The resistivity shows a field-dependent minimum at low temperature that has been explained as due to the intergrain transport phenomenon.

1. Introduction

Perovskite manganese oxides of the general formula $R_{1-x}A_xMnO_3$ (R = rare-earth metal, A = divalent element) have been extensively studied due to their colossal-magnetoresistance (CMR) effect near the Curie temperature T_C, which could be very important in device applications [1]. Replacement of an amount x of La^{3+} in antiferromagnetic $LaMnO_3$ by a divalent cation (Sr^{2+} or Ca^{2+}) gives rise to a doped mixed-valence lanthanum manganite system that is ferromagnetic in nature and exhibits metal–insulator transition at a temperature very close to the magnetic transition temperature T_C. Due to the presence of Mn^{3+}–O–Mn^{4+} pairs, the

[1] Author to whom any correspondence should be addressed.

spin dynamics and the electronic transport properties are traditionally explained in terms of the Zener double-exchange (DE) mechanism [2]. However, recent experimental findings like the Debye–Waller factor [3] and isotopic substitution T_C-shift [4] show that in addition to DE, various other factors such as the strong electron–phonon interaction [5], the charge and orbital ordering [6], the average sizes of the R and A cations [7], and the oxygen stoichiometry [8] also need to be considered. An important feature as regards these manganites is the distortion of the MnO_6 octahedron due to the Jahn–Teller effect that results in the change of the Mn–O lengths and the corresponding bond angles. Such distortion may also take place for certain ranges of values of the average radius of the R site. The metallicity and metal–insulator transition temperature show variation with the tolerance factor and average radius of the rare-earth site [7, 9].

Although detailed property–structure relationships have been studied for the divalent cation-doped $R_{1-x}A_xMnO_3$ compounds, data on monovalent cation doping [10–12] are limited. Most of the literature is devoted to the interplay between magnetic and transport properties, and less attention has been paid to the correlation between structure and magnetic properties. We have studied in detail the property–structural relationship of $La_{1-x}Na_xMnO_3$ ($0.07 \leqslant x \leqslant 0.40$). In the case of Na doping, for every amount x of Na, an amount $2x$ of Mn^{3+} will be converted to Mn^{4+}, and hence the cation valency distribution can be represented as $La^{3+}_{1-x}Na^{+}_{x}(Mn^{3+}_{1-2x}Mn^{4+}_{2x})O_3$. As a result, even a small amount of Na doping results in a large number of charge carriers and a consequent increase in the conductivity is achieved. Moreover, because of the large valency difference between Na^+ and La^{3+}, there is an increased difference in potential between the Na and the La sites although the ionic radii of La^{3+} and Na^+ are comparable. Hence one expects that study of the effect of Na doping in the manganite system will enable a better understanding of the CMR effect in these compounds to be achieved. An important point to note is the loss of Na during the sintering process [10, 11]. We have determined the difference between the actual and the nominal concentrations of Na in the sample using the atomic absorption spectroscopy technique. In this paper we report the results of x-ray diffraction (XRD), atomic absorption spectroscopy (AAS), magnetization, and electrical transport measurements of the Na-doped lanthanum manganites. The Jahn–Teller effect and tolerance factor have been discussed on the basis of the distortion of the MnO_6 octahedra and their links and orientations, and its subsequent effect on the magnetic and electrical transport properties.

2. Experimental procedure

Ceramic polycrystalline samples of $La_{1-x}Na_xMnO_3$ ($0.07 \leqslant x \leqslant 0.40$) were prepared using the conventional solid-state reaction method. Stoichiometric amounts of La_2O_3, Na_2CO_3, and MnO_2 powders were thoroughly mixed and then calcined for 12 hours at 1000 °C. The powder thus obtained was then reground, pressed into pellets, and sintered in air at 1160 °C for 20 hours. This specific temperature was chosen to get a single-phase compound without losing much Na during the sintering process. The XRD intensity data used for crystal structure analysis were collected by a Rigaku diffractometer with a 12 kW x-ray generator and Cu Kα radiation. A scanning rate of 0.015° s^{-1} was adopted and the data were taken at room temperature in the 2θ range of 20°–85°. The TREOR program [13] was used to index the XRD pattern, and refinement of the diffraction data was done using the Rietveld powder diffraction profile-fitting technique [14]. The Na content in the sample was determined using a Perkin-Elmer atomic absorption spectrophotometer. The samples were dissolved by slowly heating in 9 ml aqua regia and then transferred quantitatively into a 250 ml volumetric flask and diluted to the required volume with distilled water. The wavelength of 589.6 nm was

chosen and NaCl solutions of different concentrations were used as standards for calibrating the spectrometer. The magnetization measurements were carried out by a Quantum Design SQUID magnetometer in the temperature range 5-400 K. The samples were zero-field cooled from room temperature to 5 K and the data were taken with increasing temperature at a field of 0.1 T. The transition temperatures are taken as the maxima of $\mathrm{d}M/\mathrm{d}T$ versus temperature curves. The electrical resistivity was measured using the standard four-probe method in the temperature range 5–400 K and in the field interval 0–5.0 T.

3. Results and discussion

The analysis of the x-ray powder diffraction pattern shows the formation of homogeneous single-phase compound with rhombohedrally distorted perovskite structure in the space group $R\bar{3}c$ with coordination number $Z = 6$ in the composition range $0.07 \leqslant x \leqslant 0.20$. Figure 1 shows a typical x-ray powder diffraction pattern for $La_{0.83}Na_{0.17}MnO_3$. The crosses show the actual data and the calculated curve is superposed on them. The bottom line shows the difference between the experimental and the calculated XRD patterns. Very good agreement between the calculated and the observed data is obtained. This is evident from the values of the goodness-of-fit factor $s = 1.59$, the residual factor $R_p = 4.83\%$, and the weighted residual factor $R_{wp} = 6.32\%$. The values of R_p, R_{wp}, and s for all of the compounds are listed in table 1. The three equivalent positions (6a, 6b, and 18e) in the rhombohedral unit cell are occupied by 6 (La, Na), 6 Mn, and 18 O respectively. We mention here that we have not carried out an explicit determination of the oxygen content, but because of the close agreement of our result with published results, we consider our composition to be reasonably correct. The AAS results show that at lower concentrations most of the Na remains in the sample while at higher concentrations a small amount of Na loss is observed. The actual amount of Na present in the sample as measured by AAS is given in table 1. Our XRD spectra do not show any

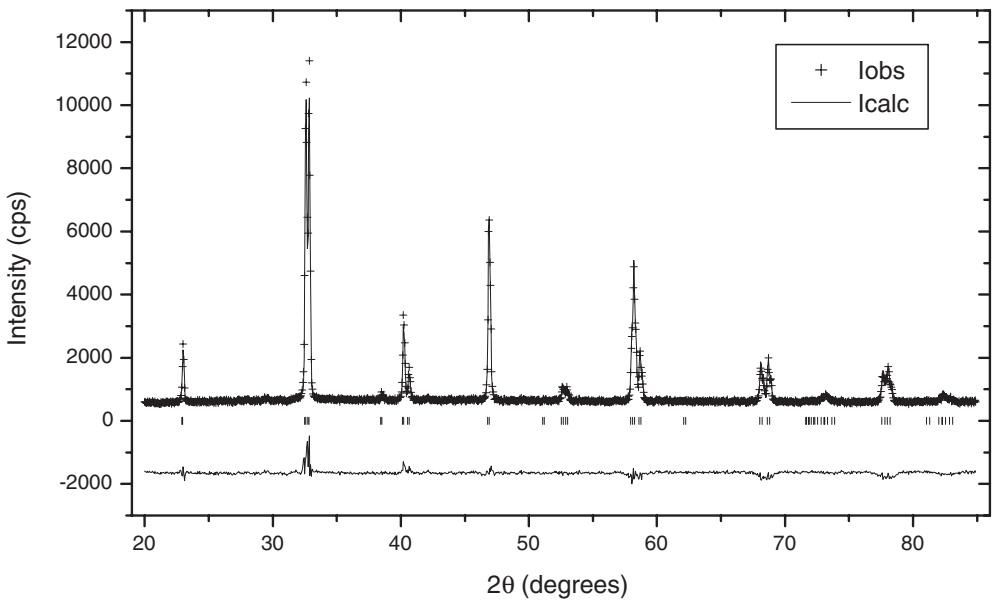

Figure 1. The x-ray diffraction pattern of $La_{0.83}Na_{0.17}MnO_3$. The bottom line shows the difference between the experimental and the fitted curve.

Table 1. Structure, magnetic, and transport properties of $La_{1-x}Na_xMnO_3$ ($0.07 \leqslant x \leqslant 0.40$). T_C and T_{im} are the magnetic and metal–insulator transition temperatures. a and c are the lattice parameters for the rhombohedral crystal structure. The bond lengths and bond angles correspond to each unit cell. M_S is the maximum magnetization at 10 K. R_p, R_{wp}, and s are the residual factor, the weighted residual factor, and the goodness-of-fit factor respectively.

Nominal composition x	0.07	0.10	0.13	0.17	0.20	0.30	0.40
Measured Na content	0.079	0.115	0.136	0.152	0.167	0.272	0.373
T_C (K)	220	278	292	306	310	327	330
T_{im} (K)	194	299	301	322	330	328	
a (Å)	5.524(3)	5.519(8)	5.517(6)	5.508(2)	5.497(1)	5.493(1)	5.495(3)
c (Å)	13.346(9)	13.35(1)	13.348(2)	13.342(1)	13.331(1)	13.327(1)	13.331(8)
Unit-cell volume (Å^3)	352.7(5)	352.2(8)	351.9(3)	350.5(7)	348.8(7)	348.2(6)	348.6(6)
Mn–O–Mn bond angle (deg)	164.33	163.58	163.94	164.39	164.19	165.76	167.01
Mn–O bond length (Å)	1.963	1.964	1.959	1.961	1.956	1.951	1.949
(La, Na)–O bond length (Å)	2.495	2.479	2.480	2.493	2.480	2.505	2.527
Tolerance factor t	0.893	0.893	0.895	0.899	0.897	0.908	0.917
M_S at 10 K (emu g^{-1})	87.99	89.52	88.76	87.35	83.65	81.3	73.67
R_p (%)	3.99	4.67	4.78	4.83	3.83	4.38	4.39
R_{wp} (%)	5.20	5.99	6.27	6.32	4.89	5.67	5.96
s	1.45	1.50	1.76	1.59	1.38	1.51	1.96

systematic increase of impurity peaks even at high Na concentration (figure 2(a)). However a closer inspection of the XRD spectra shows a progressive change in the peak shapes with increasing Na content (figure 2(b)). The doublet peaks seen at low Na compositions get closer with increasing Na content and are reduced significantly for $x \geqslant 0.20$. A detailed Rietveld refinement shows the onset of an orthorhombic phase for $x \geqslant 0.20$ which increases with increasing Na content. It may be noted that there may be different reasons for the formation of a second structural phase, such as a doping effect or multiple occupancy of Na in both La and Mn sites, and a detailed analysis of the phase and occupancy of $La_{1-x}Na_xMnO_3$, $x \geqslant 0.20$, is being carried out.

Figure 3(a) shows the variations of the lattice parameters a and c with the concentration of Na in $La_{1-x}Na_xMnO_3$ ($0.07 \leqslant x \leqslant 0.40$). The lattice parameters decrease from $a = 5.524(3)$ Å to 5.495(3)Å and $c = 13.346(9)$ Å to 13.331(8) Å with increasing Na concentration. A clear change of slope for the lattice parameter is seen at $x \geqslant 0.20$ indicating the possible presence of a second crystal phase. A similar feature is observed for the unit-cell volume as shown in figure 3(b), indicating that the lattice shrinks and the unit cell becomes smaller with increasing Na concentration. This is due to the smaller size of the Na^+ ion (113 pm) as compared to the La^{3+} ion (117.2 pm). The lattice parameters and the cell volume at different concentrations of Na are given in table 1. The variations of the Mn–O–Mn bond angle and the tolerance with the Na concentration are shown in figure 4(a). Both the bond angle and the tolerance show an increasing trend with increasing Na content. Due to the Jahn–Teller effect, the MnO_6 octahedron gradually gets more distorted with increased doping. But for a particular Na concentration, no significant change could be observed in the six Mn–O–Mn bond angles in a unit cell. This indicates that there is no buckling of the MnO_6 octahedra and no static Jahn–Teller effect. However, the tolerance, which gives a measure of the difference between the (La, Na)–O and the Mn–O bond lengths, increases with increasing Na content. The decrease in the bond-length difference is due to the decrease in lattice parameter and the distortion of the MnO_6 octahedron with increasing Na content in the compounds. In figure 4(b), the Mn–O–Mn

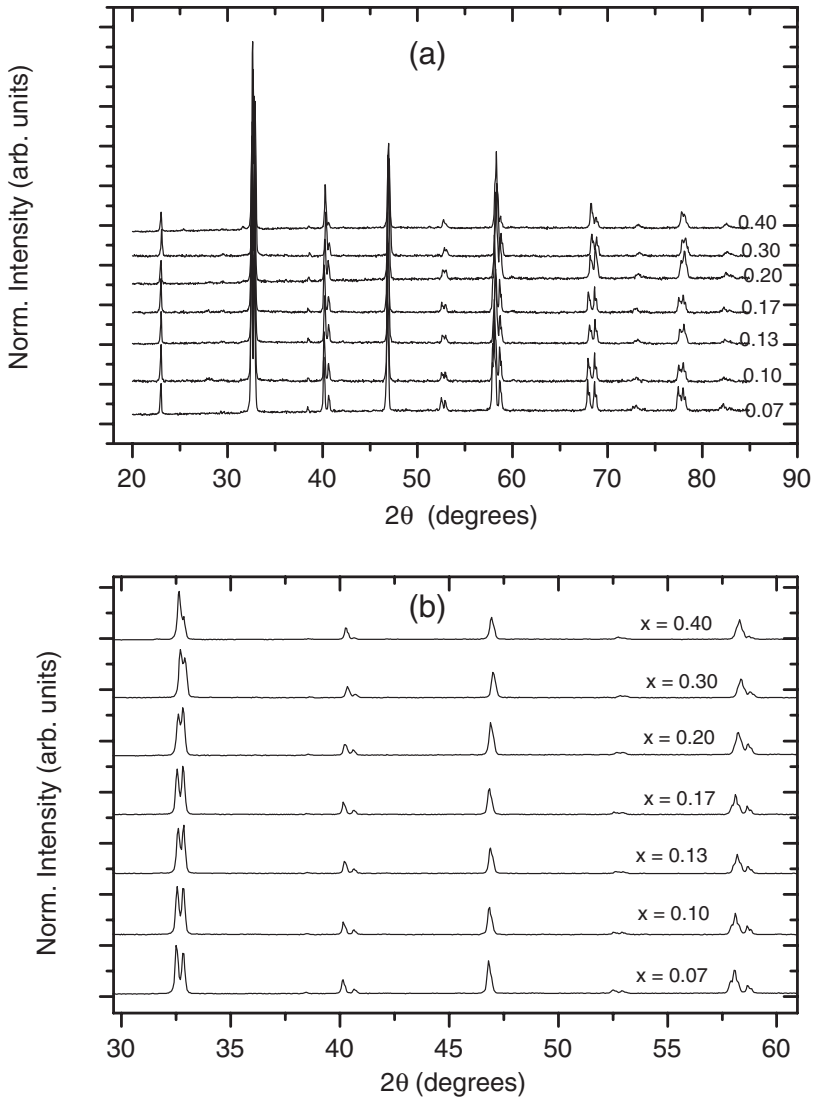

Figure 2. (a) The XRD pattern of $La_{1-x}Na_xMnO_3$, $x = 0.07$–0.40. (b) The XRD pattern of the first four highest-intensity peaks. Note the variation of the peak shapes with composition.

bond angle is plotted against the tolerance factor t. The bond angle increases almost linearly with the tolerance in the composition range $0.07 \leqslant x \leqslant 0.40$. Thus as a function of Na content, the distortion of the MnO_6 octahedron becomes less with the Mn–O–Mn bond angle moving toward 180°, the structure tending to become more cubic ($t = 1$). One of the likely reasons is that with increased doping the average size at the La site reduces, resulting in the La–O distance increasing or at least remaining the same. But the Mn–O distance reduces. The overall effect of this is that the tolerance factor, which is given as the ratio of these two distances, increases. High Na content drives the structure to become more cubic, resulting in an increase of the one-electron bandwidth. Consequently there is a greater overlap between the O 2p and Mn 3d orbital, resulting in an increased hopping interaction. Hence at higher

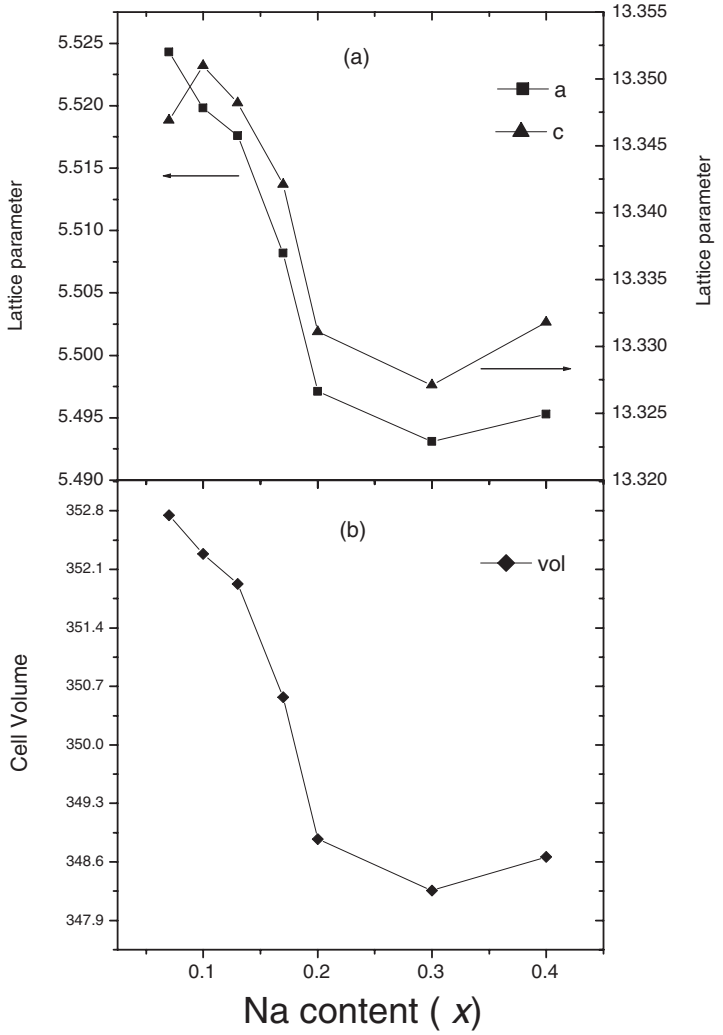

Figure 3. (a) Lattice parameters a and c versus concentration of Na. (b) Variation of the unit cell with the concentration of Na.

Na content an increase of conductivity should be observed. A satisfactory result has been obtained from the magnetic and electrical transport property measurements. The values of the Mn–O–Mn angle, Mn–O, (La, Na)–O bond lengths, and the tolerance are listed in table 1.

Figure 5 shows the magnetization versus temperature data for $La_{1-x}Na_xMnO_3$ ($0.07 \leqslant x \leqslant 0.40$). A ferromagnetic-to-paramagnetic transition occurs for all of the compounds. A small glitch seen at a temperature of 43 K is most probably due to some unreacted MnO_2 powder. Unlike for the strontium-doped or calcium-doped lanthanum manganites, in this case the T_C-value increases for low Na doping but tends to saturate for $x \geqslant 0.20$. A possible explanation is the completion of the rhombohedral phase that contributes to the magnetization and development of the orthorhombic phase that hinders the magnetization. Thus for $x \leqslant 0.20$ the situation is very similar to the divalent-metal-doping case, but above $x = 0.20$ the presence of both rhombohedral and orthorhombic structure makes the case different from

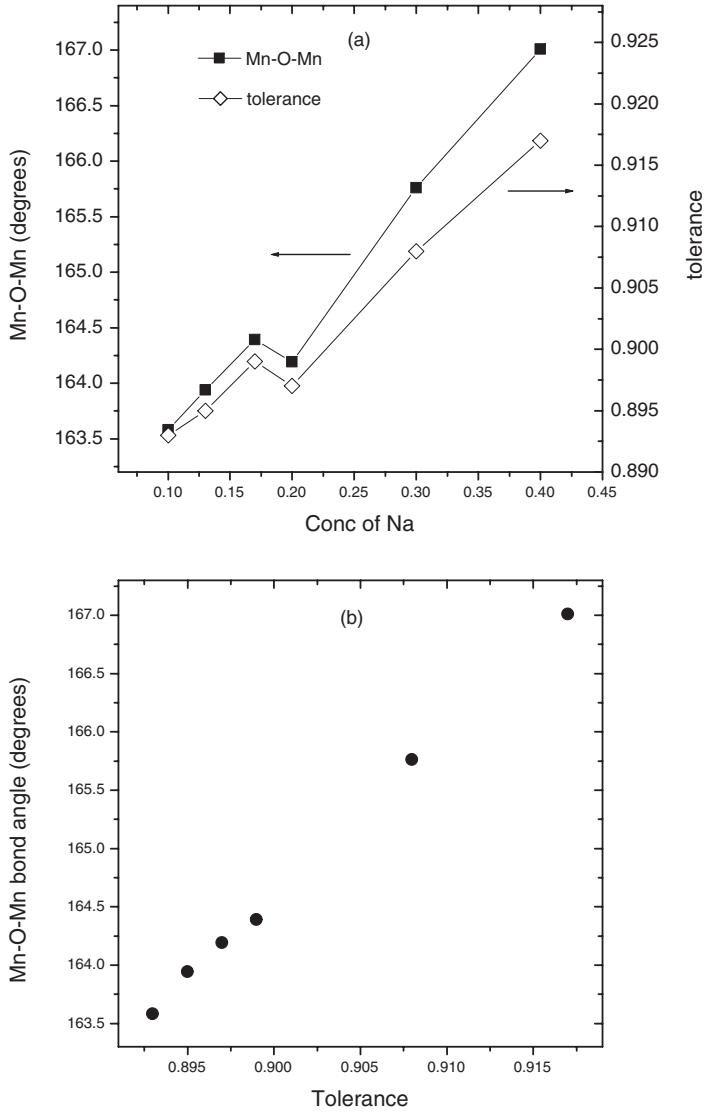

Figure 4. (a) Mn–O–Mn bond angle and tolerance versus Na concentration. (b) The Mn–O–Mn bond angle plotted against the tolerance.

the divalent metal case. Now the buckling effect may become important and may affect the magnetization. Hence we suggest that these two competing phases balance each other in the region $0.20 \leqslant x \leqslant 0.40$, resulting in T_C-saturation. The T_C-values are listed in table 1. The inset of figure 5 shows the saturation magnetization (M_S) at 5 T versus concentration x at 10 K. The M_S-value increases for lower doping values until it attains a peak and then decreases for higher concentration of Na. The variation of the values of T_C and M_S cannot be interpreted in terms of the double-exchange (DE) mechanism alone. Considering that x Na ions produce $2x$ holes, in the low-doping regime the Mn^{3+}/Mn^{4+} ratio is favourable to ferromagnetism. However, as the doping level increases, the concentration of Mn^{4+} exceeds that of Mn^{3+}, thereby resulting in there being fewer Mn^{3+}–O–Mn^{4+} pairs. This weakens the

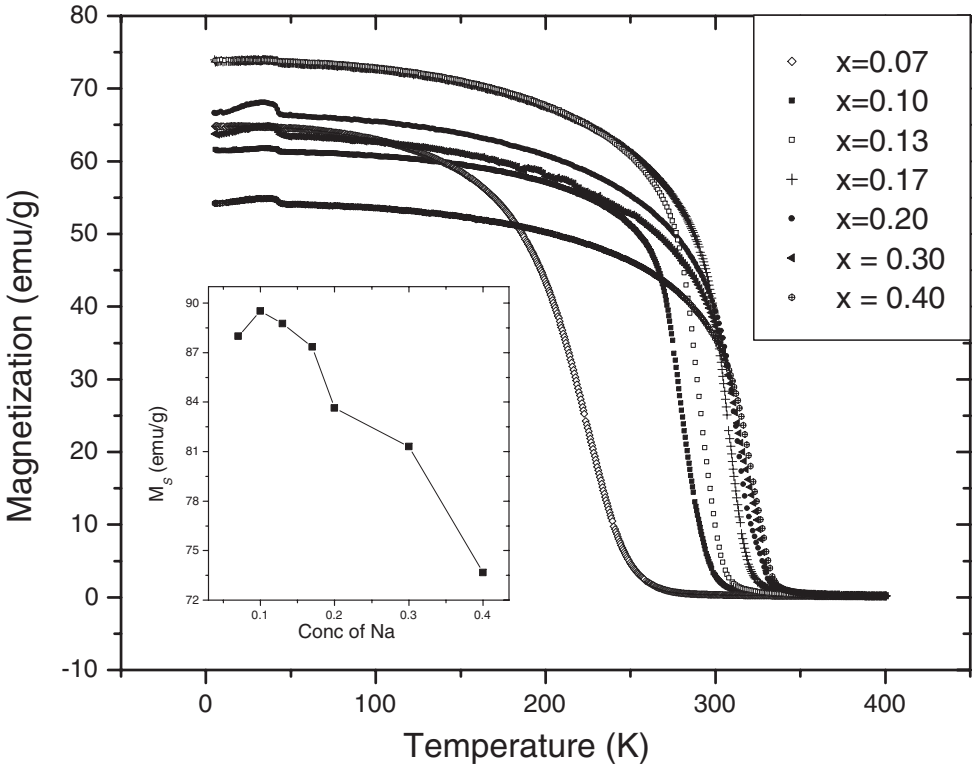

Figure 5. Magnetization versus temperature curves for $La_{1-x}Na_xMnO_3$, $x = 0.07$–0.40, at 1000 G. The inset shows a plot of the maximum magnetization M_S at 5 T at 10 K versus the Na concentration.

DE interaction and favours Mn^{4+}–O–Mn^{4+} superexchange interaction. The result is that the magnetization is weakened and there is little increase of the transition temperature. But with increase of the Na content, the Mn–O–Mn bond angle and the tolerance increase, resulting in an increase in the hopping interaction and hence also an increase in the T_C-value. Thus there is a competition between the Mn^{4+}–O–Mn^{4+} superexchange interaction and the hopping interaction. In the high-doping regime, due to higher Mn^{4+} concentration the superexchange contribution becomes significant as compared to the hopping interaction, and so the change of the transition temperature is small.

Figure 6 shows the variation of the electrical resistivity with temperature at zero field. All the compounds show a metallic behaviour below a temperature T_{im} and above it behave like insulators. A drastic drop in the absolute value of the resistivity is observed when the Na doping changes from 7% to 10%. The metal–insulator transition temperature T_{im} increases with the Na concentration x. The variation of the metallic conductivity with doping can be explained by the fact that there are twice as many Mn^{4+} ions as there are Na ions and each of these Mn^{4+} will contribute a hopping hole. Thus for small Na concentration there are enough holes in the e_g band that will contribute to the conductivity. Therefore even for 7% Na a distinct metallic region is observed below T_{im}. The conductivity increases as the Na content increases because of the increase in the number of holes. The resistivity is small at low temperature and increases with increasing temperature due to increasing thermal frustration of the spins. Above T_{im} the Jahn–Teller-type distortion present in the unit cell traps the charge carriers and

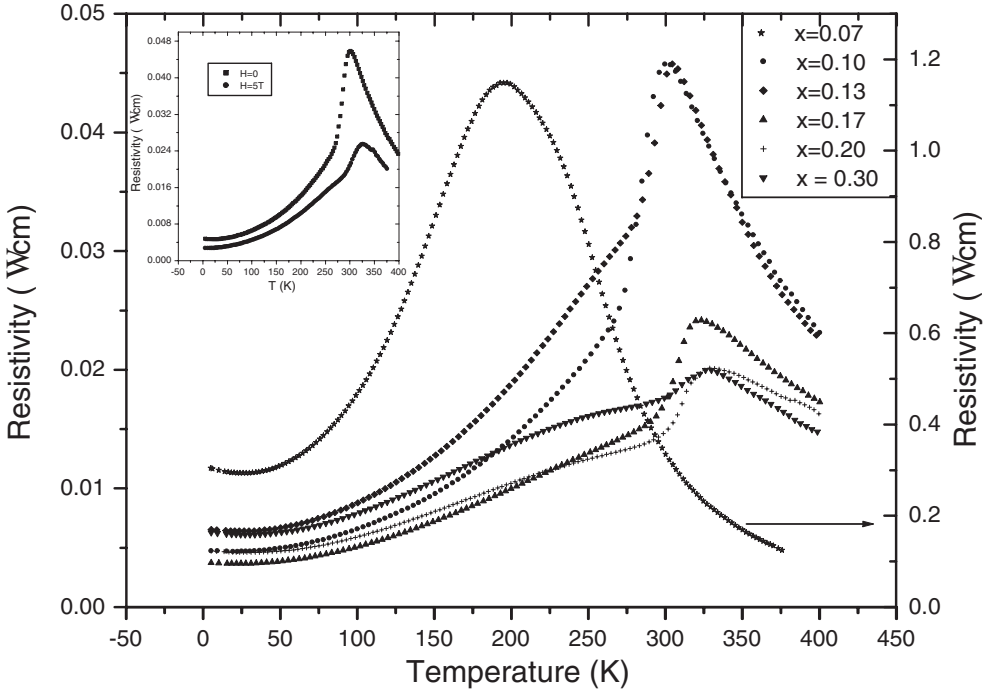

Figure 6. Zero-field resistivity versus temperature curves of $La_{1-x}Na_xMnO_3$, $x = 0.07$–0.20. The inset shows the resistivity versus temperature curve of $La_{0.90}Na_{0.10}MnO_3$ at 0 and 5 T applied field.

gives rise to polarons. Hence above T_{im} the resistivity shows a polaronic-type behaviour. In the inset of figure 6 we show the resistivity versus temperature for $La_{0.90}Na_{0.10}MnO_3$ at 0 and 5 T field. A drastic decrease in resistivity is observed when an external field is applied. The application of field results in spins getting favourably oriented as a result of which the charge carriers suffer less scattering during the hopping process and hence the resistivity decreases. There is a shift in the change in the peak by 20 K and this is most probably due to stronger interaction between the Mn^{3+} and Mn^{4+} spins. A maximum magnetoresistance ratio of 45% is observed at a temperature of 300 K which is higher than that for $La_{1-x}Sr_xMnO_3$ with a similar x-value.

The low-temperature resistivity behaviour of some selected samples is shown in figure 7. A distinct resistive minimum is observed in the temperature range 20–30 K. Neither the resistive minimum temperature nor the depth of the minimum is sensitive to the doping effect. Thus the minimum does not seem to be affected by the lattice shrinkage due to Na doping in the La site. However, when a field of 5 T is applied, the minimum disappears (figure 8(a)). Above the minimum temperature, the resistivity is governed by a power law ($\rho \sim AT^2$, $T \leqslant 230$ K) as shown in figure 8(b). A strong electron–electron scattering resulting in a change in the density of states near the Fermi energy has been suggested for the resistive minimum [15]; but such reasoning cannot explain the disappearance of the minima due to an applied field. Recently Furukawa [16] has argued that at low temperature, spin-fluctuation scattering is much stronger and $\rho \sim AT^3$ behaviour should be observed. We have not observed $\rho \sim T^3$, most probably because our sample is polycrystalline while Furukawa deals with single crystal. An alternative explanation is the transport across the grain boundaries that are extremely sensitive to the

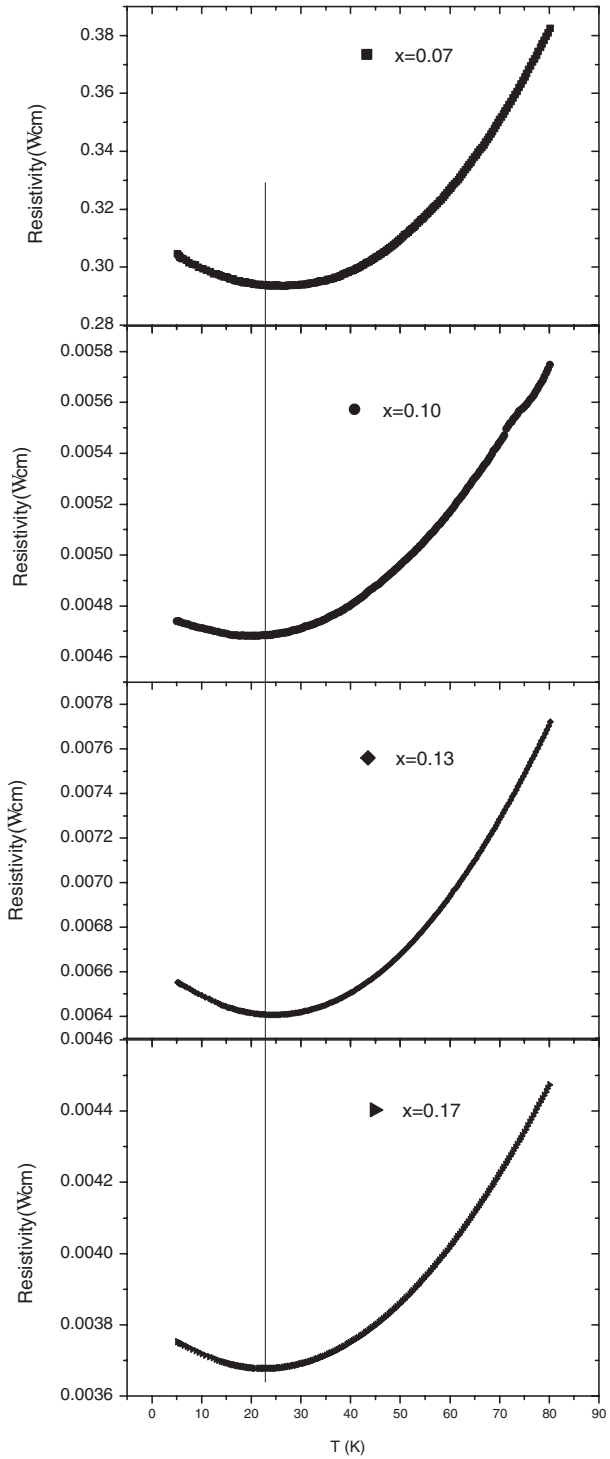

Figure 7. The low-temperature resistivity versus temperature curve of $La_{1-x}Na_xMnO_3$, $x = 0.07$–0.17. A clear minimum in the curve can be seen.

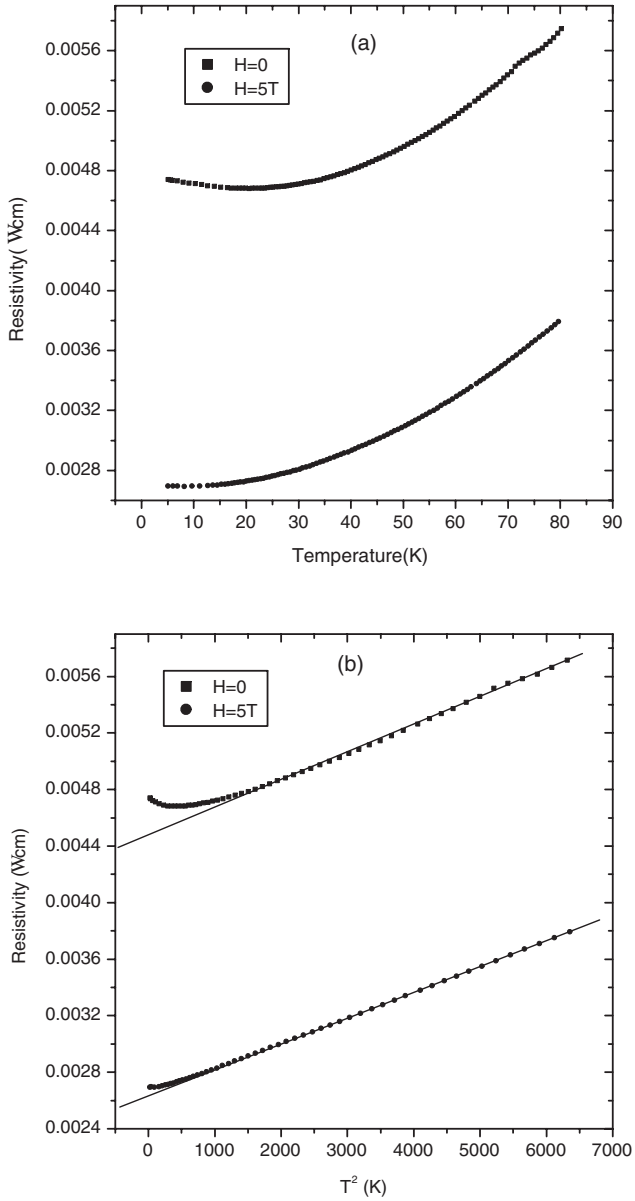

Figure 8. (a) The effect of a 5 T field on the resistivity minimum of $La_{0.90}Na_{0.10}MnO_3$. (b) A plot showing the $\rho \sim T^2$ behaviour for $La_{0.90}Na_{0.10}MnO_3$.

applied field, as studied by Rozenberg *et al* [17]. In the absence of any external magnetic field, the neighbouring grains align in such a way that the charge carriers in them have opposite spins and cannot move if the spin is to be conserved. Due to such an antiferromagnetic interaction, there exists a gap between the charge carriers of the neighbouring grains. As the temperature increases, the grains, due to thermal energy, orient themselves and also the carriers gain enough thermal energy to overcome this barrier. Thus there is a decrease of the resistivity with increasing temperature. But superposed on this is the net metallic resistivity

due to the bulk system. Hence due to both these contributions a minimum is seen at low temperatures. Application of the field causes the grains to orient in such a way that the carrier spins from the neighbouring grains align themselves favourably and the energy gap reduces, and accordingly the minimum also reduces with increasing applied field. In order to explain the $\rho \sim AT^2$ behaviour, a Baber-type electron–electron scattering mechanism is considered by several authors [18, 19]. However, in the temperature range $30 \leqslant T \leqslant 230$ K, pure electron–electron scattering seems unlikely. Also no large increase of γ in this temperature range is reported, although one would expect that to arise. On the other hand, a $\rho \sim AT^2$ behaviour in a ferromagnet has been reported as due to magnon excitation [20]. Thus probably the $\rho \sim AT^2$ behaviour is due to electron–spin scattering. According to this model, the ferromagnetism is mainly due to the Hund's coupling that results in the spin alignment of the charge carriers, and the number of electrons in the d band is non-integral—a fact that is obvious for the manganites following the DE theory.

4. Conclusions

The complex interplay among the structure, magnetic, and electrical transport properties of Na-doped lanthanum manganite has been studied in detail. The unit-cell volume decreases with increase in sodium content. As a result, the difference between the (La, Na)–O and Mn–O bonds decreases and the structure becomes more cubic. This enhances the hopping interaction and so an increase in the conductivity is observed. Also an increased amount of Na leaves an increased number of holes in the e_g band of Mn, so there are effectively more charge carriers. However, since each Na results in two holes in the e_g band, the maximum magnetization is obtained at $\simeq$12% of Na since at this concentration of Na the Mn^{3+}/Mn^{4+} ratio is favourable for getting maximum CMR. The resistivity curves show metal–insulator transition in the composition range $0.07 \leqslant x \leqslant 0.30$. Application of magnetic field results in drastic change of the electrical resistivity near T_C and a magnetoresistance ratio of 45% is observed for the 10% Na-doped compound. In the paramagnetic region the transport is of polaronic type, but in the ferromagnetic region, along with metallic conductivity, at low temperature a resistivity minimum is observed along with a T^2-dependence of the resistivity. While the $\rho \sim T^2$ behaviour is due to the electron–spin scattering effect, the minima are due to the intergrain tunnelling effect. The neighbouring grains usually show antiferromagnetic interaction, and scattering of the charge carriers at the grain boundaries can give rise to effects that are very sensitive to external applied magnetic field.

Acknowledgments

This work was supported by the Consortium for Advanced Radiation Sources, University of Chicago. The authors wish to thank Dr Billy Fairless of the Department of Chemistry, SIUC, for helping in the AAS experiment.

References

[1] Tokura T (ed) 2000 *Colossal Magneto-Resistive Oxides* (New York: Gordon and Breach)
[2] Zener C 1951 *Phys. Rev.* **81** 440
[3] Dai P, Zhang J, Mook H A, Liou S J, Dowben P A and Plummer E W 1994 *Phys. Rev.* B **54** 3694
[4] Zhao G, Conder K, Keller H and Muller K A 1996 *Nature* **381** 676
[5] Millis A J, Littlewood P B and Shraiman B I 1995 *Phys. Rev. Lett.* **74** 5144
[6] Chen C H and Cheong S-W 1996 *Phys. Rev. Lett.* **78** 4253

[7] Hwang H Y, Cheong S-W, Radaelli P G, Marezio M and Battlogg B 1995 *Phys. Rev. Lett.* **75** 914
[8] Mitchell J F, Argyriou D N, Potter C D, Hinks D G, Jorgensen J D and Bader S D 1996 *Phys. Rev.* B **54** 6172
[9] Sun J R, Rao G H and Liang J K 1997 *Appl. Phys. Lett.* **70** 1900
[10] Itoh M, Shimura T, Yu J D, Hayashi T and Inaguma Y 1995 *Phys. Rev.* B **52** 12 522
[11] Rao G H, Sun J R, Barner K and Hamad N 1999 *J. Phys.: Condens. Matter* **11** 1523
[12] Boudaya C, Laroussi L, Dhahri E, Joubert J C and Cheikh-Rouhou A 1998 *J. Phys.: Condens. Matter* **10** 7485
[13] Winner P E 1965 *J. Appl. Crystallogr.* **9** 594
[14] Rietveld H M 1969 *J. Appl. Crystallogr.* **2** 65
[15] Tiwari A and Rajeev K P 1999 *Solid State Commun.* **111** 33
[16] Furukawa N 2000 *J. Phys. Soc. Japan* **69** 1954
[17] Rozenberg E, Auslender M, Felner I and Gorodetsky G 2000 *J. Appl. Phys.* **88** 2578
[18] Abdelmoula N, Cheikh-Rouhou A and Reversat L 2000 *J. Phys.: Condens. Matter* **13** 449
[19] Urushibara A, Moritomo Y, Arima T, Asamitsu A, Kido G and Tokura Y 1995 *Phys. Rev.* B **51** 14 103
[20] Mott N F 1974 *Metal–Insulator Transitions* (London: Taylor and Francis)